Journal of the Optical Society of America B
OPTICAL PHYSICS

Ab-initio design of realistic Fabry–Perot cavities for accurate refractive index determination of liquids and gases

J. G. Munguia-Fernandez,[1] V. Sanchez,[1] and C. Wang[2,*]

[1]Departamento de Física, Facultad de Ciencias, Universidad Nacional Autónoma de México, Mexico City, Mexico
[2]Instituto de Investigaciones en Materiales, Universidad Nacional Autónoma de México, Mexico City, Mexico
*Corresponding author: chumin@unam.mx

Received 6 March 2018; revised 5 July 2018; accepted 11 August 2018; posted 13 August 2018 (Doc. ID 325420); published 7 September 2018

Fabry–Perot cavities (FPCs) provide a simple and precise alternative to measure the refractive indices of gases and liquids. The performance of an FPC is very sensitive to the quality of its dielectric multilayer mirrors. In this article, a combined *ab-initio* and transfer-matrix study is carried out for a realistic Fabry–Perot microcavity made of TiO_2/SiO_2, including interface atomic diffusions and possible layer thickness variations. The refractive indices obtained from the density functional theory are used as the input of cavity transmittance calculations. The performance of such a Fabry–Perot cavity is monitored by the quality factor, finesse, and full width at half maximum (FWHM) of its main resonant peaks. The results confirm the exponential decrease of FWHM with the number of layers and then an exponential growth of the finesse. An analytical solution for the optical transmittance of few-layer cavities is also presented. Furthermore, the results reveal non-uniform shifts of the resonant peaks, due to the presence of a finite-layer interface width or layer thickness fluctuation. Finally, simulated measurements of the refractive indices of CO_2 and ethanol by using this *ab-initio* designed realistic Fabry–Perot microcavity are analyzed in detail.

OCIS codes: (050.2230) Fabry-Perot; (140.3948) Microcavity devices; (310.4165) Multilayer design; (050.5298) Photonic crystals.

https://doi.org/10.1364/JOSAB.35.002368

1. INTRODUCTION

Recent developments of thin-film Fabry–Perot (FP) photonic resonant microcavities have attracted considerable attention [1–3]. Such FP cavities (FPCs) consist of a central planar defect placed between two dielectric multilayer mirrors made of a periodic arrangement by alternating high and low refractive index materials with a quarter-wave thickness. The transmission spectrum of these cavities contains a narrow high-transmittance resonant peak, whose full width at half maximum (FWHM) exponentially decreases with the number of layers in the mirror [2]. This fact can be used for an accurate and real-time determination of the refractive indices of liquids and gases found in the planar defect.

In general, the quality of an FPC can be evaluated by means of the parameters, such as FWHM, the spacing between two nearest neighboring transmission maxima called free spectral range (FSR) [4], and the finesse of an FPC given by [5]

$$\text{Finesse} = \frac{\text{FSR}}{\text{FWHM}}. \tag{1}$$

From the theoretical point of view, the design of an FPC with a high finesse value depends essentially on the refractive-index contrast of dielectric multilayer mirrors, the number of layers, and the variation of these refractive indices with the wavelength. For an FPC operating in the visible region, these dielectric layers should additionally possess a wide electronic band gap. Nowadays, the rapid development of *ab-initio* quantum calculation methods provides an alternative way to search proper materials to build an accurate FPC. In this article, we report an *ab-initio* study of a realistic FPC for the optical refractive index detection of gases or liquids.

2. MODELING FABRY–PEROT CAVITIES

For one-dimensional photonic devices, the transfer matrix method has been a simple and powerful tool to study the propagation of electromagnetic waves in multilayer structures. Such propagation through each layer can be divided into two parts: (1) the transmission within each layer and (2) the wave refraction at the layer–layer interface. The former is described by the transfer matrix (P_j) of layer j given by [4]

$$P_j = \begin{pmatrix} \cos\delta_j & -\sin\delta_j \\ \sin\delta_j & \cos\delta_j \end{pmatrix}, \tag{2}$$

where $\delta_j = 2\pi n_j d_j \cos\theta_j/\lambda$, λ is the wavelength, θ_j is the refraction angle determined by Snell's law, and n_j and

d_j are, respectively, the refractive index and thickness of layer j, while the latter is characterized by

$$B_{j+1|j} = \begin{pmatrix} 1 & 0 \\ 0 & q_{j+1|j} n_{j+1}/n_j \end{pmatrix}, \quad (3)$$

where $q_{j+1|j} = \cos\theta_{j+1}/\cos\theta_j$ for the polarization s or transverse electric (TE) mode and $q_{j+1|j} = \cos\theta_j/\cos\theta_{j+1}$ for the polarization p or transverse magnetic (TM) mode [4]. Hence, the resulting transfer matrix (M) of N layers can be written as

$$M = \begin{pmatrix} m_{11} & m_{12} \\ m_{21} & m_{22} \end{pmatrix} = B_{N+1|N} \prod_{j=1}^{N} P_j B_{j|j-1}, \quad (4)$$

where $j = 0$ and $j = N + 1$ correspond the boundary media of the multilayer, being usually vacuum or air. Then, the transmittance (T) of this multilayer is given by [6]

$$T = \frac{4}{(m_{11} + m_{22})^2 + (m_{12} - m_{21})^2}. \quad (5)$$

Figure 1 shows the transmittance (T) with normal incidence as a function of λ_0/λ for (a) an FPC of nine layers as illustrated in its inset and (b) three FPCs of 21 (red circles), 41 (green squares), and 61 (violet triangles) layers, where all FPCs are placed in vacuum and made of a central defect (D) with a thickness of $d_D = 1500$ nm and a refractive index of $n_D = 1.0$ surrounded by two periodic dielectric mirrors built by low (A) and high (B) refractive index layers with $n_A = 1.5$ and $n_B = 2.5$, whose thicknesses are $d_A = 250$ nm and $d_B = 150$ nm, respectively. The quantities of FWHM and FSR are also indicated in Fig. 1(a).

There is an analytical solution of the transmittance for the nine-layer FPC given by

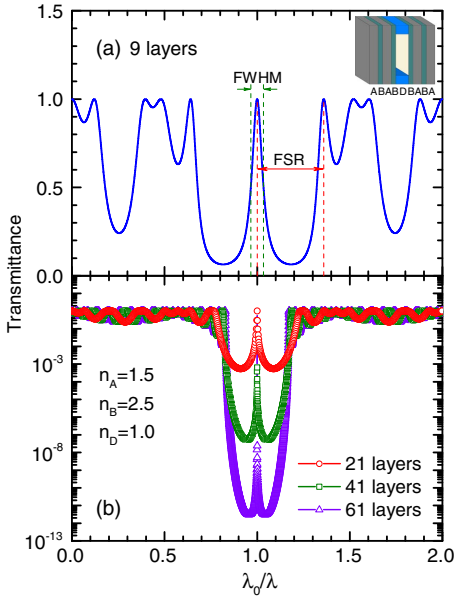

Fig. 1. Transmittance (T) versus the inverse of wavelength (λ_0/λ) for (a) Fabry–Perot cavity (FPC) of nine layers and (b) FPCs of 21, 41, and 61 layers.

$$T = \frac{4}{(V \sin\delta_D + R\cos\delta_D)^2 + (W \sin\delta_D + Z\cos\delta_D)^2}, \quad (6)$$

where

$$V = -2(\alpha+\gamma)\beta(\alpha^2\Omega - \beta^2 - \beta^2\Omega\xi^2 + \gamma^2\Omega^2\xi^2)\Omega^{-2}\xi^{-1}, \quad (7)$$

$$R = 2[\beta^4 - 2(\alpha\gamma + \alpha^2 + \gamma^2)\beta^2\Omega + \alpha^2\gamma^2\Omega^2]\Omega^{-2}, \quad (8)$$

$$W = -[\beta^4 - 2\alpha^2\Omega\beta^2 + \alpha^4\Omega^2 - \beta^2(\alpha+\gamma)^2\Omega^2(n_A^2 - \xi^2) + \Omega^2 n_A^2\xi^2(\beta^4 - 2\beta^2\gamma^2\Omega + \gamma^4\Omega^2)]n_A^{-1}\Omega^{-3}\xi^{-1}, \quad (9)$$

and

$$Z = -2\beta(\alpha+\gamma)(\alpha^2\Omega - \beta^2 - \Omega\beta^2 n_A^2 + \gamma^2\Omega^2 n_A^2)\Omega^{-2}n_A^{-1}, \quad (10)$$

with $\alpha = \cos^2[\pi\lambda_0/(2\lambda)] - \Omega\sin^2[\pi\lambda_0/(2\lambda)]$, $\beta = 0.5(1+\Omega)\sin(\pi\lambda_0/\lambda)$, $\gamma = \cos^2[\pi\lambda_0/(2\lambda)] - \Omega^{-1}\sin^2[\pi\lambda_0/(2\lambda)]$, $\xi = n_D/n_B$, and $\Omega = n_B/n_A$. Moreover, notice in Fig. 1(b) that the minimal values of T around the main peak at $\lambda = \lambda_0$ and its FWHM both decrease with the number of layers in the FPC.

In Fig. 2, we plot the dependence of (a), (c) FWHM and (b), (d) finesse (a), (b) on the number of layers (N) and (c), (d) on the refractive index of central defect (n_D) for the FPCs up to 113 layers with the same layer parameters as Fig. 1 and resonant peaks around $\lambda = 500$ nm (red open circles) and $\lambda = 1500$ nm (blue open squares). Figures 2(c) and 2(d) are obtained from the FPC of 113 layers.

Notice in Fig. 2(a) that the FWHM of both peaks exponentially decreases with N, and the width of peak at $\lambda = 500$ nm is always smaller than that of the peak at $\lambda = 1500$ nm, where the former grows faster than the latter with n_D, as illustrated in Fig. 2(c). Observe in Fig. 2(b) the extremely high value of

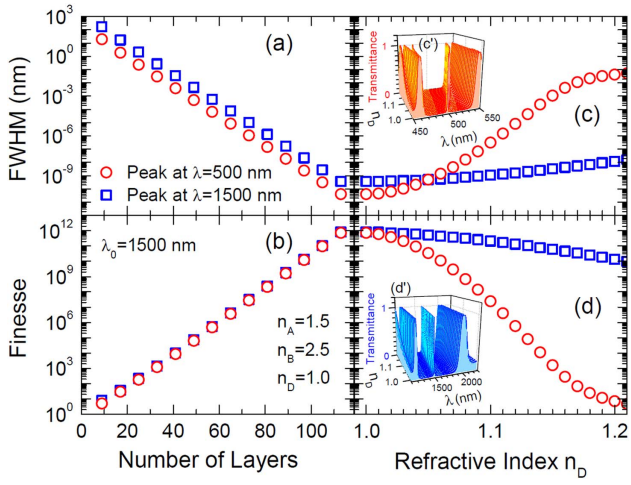

Fig. 2. (a), (c) Full width at half maximum (FWHM) and (b), (d) finesse as functions of (a), (b) number of layers and (c, d) refractive index of central defect (n_D) for (a), (b) FPCs from nine to 113 layers and (c), (d) FPC of 113 layers with $\lambda_0 = 1500$ nm for resonant peaks around $\lambda = 500$ nm (red open circles) and $\lambda = 1500$ nm (blue open squares). Insets (c'), (d'), respectively, illustrate transmittance spectra around 500 nm and 1500 nm for an FPC of 21 layers with different values of n_D.

finesse ($\sim 10^{12}$) for an FPC of 113 layers, and it decreases with n_D, being faster than that associated with the peak of 500 nm because the finesse is inversely proportional to the FWHM.

Insets (c') and (d') in Fig. 2 show the transmittance spectra, respectively, around 500 nm and 1500 nm for an FPC of 21 layers. Note the remarkable shift in the peak at 500 nm towards long wavelength, while its FWHM grows when the refractive index of the central defect n_D increases from 1 to 1.2.

3. *AB-INITIO* CALCULATIONS

The density functional theory (DFT) is currently the most used *ab-initio* method to calculate electronic and structural properties of molecules and solids. In this article, the DFT calculations were carried out by using the CASTEP code [7] within the Biovia Materials Studio, in which the same parameters of Ref. [8] were used, except that on-site Coulomb electron–electron interaction parameters of $U_d = 7$ eV and $U_p = 2$ eV are, respectively, used for d- and p-orbital electrons in TiO_2 [9], and a scissor operator of 3.1 eV is considered for SiO_2 in order to produce a correct band gap of 9 eV [10]. In general, the local density approximation (LDA) underestimates the band gap by 30%–50% [11], but it gives the correct sum rule for the exchange-correlation hole, leading to properly calculated optical properties [12]. The resulting real (n, red open circles) and imaginary (k, green open squares) parts of the refractive index corresponding to TiO_2 and SiO_2 are, respectively, presented in Figs. 3(a) and 3(b), whose atomic unit cells and electronic band structures are shown in their insets. Observe that the TiO_2 rutile phase has an almost direct band gap of 3.2 eV and a refractive index with $n \approx 2.5$ and $k \approx 0$ for $\lambda > 400$ nm, while the SiO_2 α-quartz phase possesses an indirect band gap of 9 eV and a refractive index with $n \approx 1.42$ and $k \approx 0$ for $\lambda > 140$ nm. The relationship $n(\lambda)$ obtained from *ab-initio* calculations for TiO_2 and SiO_2 will be used in the next section as the input of FPC transmittance calculations.

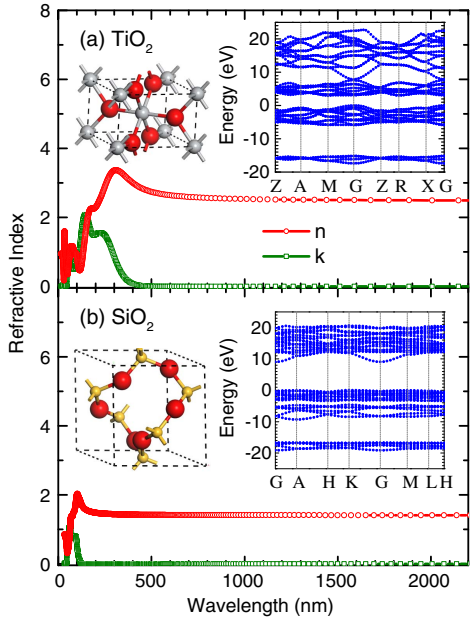

Fig. 3. Real (n, red open circles) and imaginary (k, green open squares) parts of the refractive index versus wavelength (λ) for (a) TiO_2 rutile and (b) SiO_2 α-quartz phases, whose atomic unit cells and electronic band structures are shown in their insets.

4. IMPERFECT FABRY–PEROT CAVITIES

In this section, we study the effects of atomic diffusion at layer interfaces and of systematic layer-thickness mistakes during the multilayer fabrication on the light transmission spectrum of FPC. To consider the atomic diffusion, we introduce a layer interface width (Δ_I), where the refractive index changes linearly with the position instead of an abrupt variation. For the possibility of a systematic layer-thickness mistake, we add an extra constant layer thickness (Δ_d) to each layer of the FPC, which leads to layer thicknesses of $d_A = \Delta_d + \lambda_0/[4n_{SiO_2}(\lambda_0)]$ and $d_B = \Delta_d + \lambda_0/[4n_{TiO_2}(\lambda_0)]$ with $n_{SiO_2}(\lambda_0 = 1500\ \text{nm}) \approx 1.4121$ and $n_{TiO_2}(\lambda_0 = 1500\ \text{nm}) \approx 2.5032$.

Figure 4(a) shows the light transmission spectrum for an FPC of 21 layers without any structural imperfection like that in Fig. 1(b), except for the use of *ab-initio* wavelength-dependent refractive indices $n_A(\lambda)$ and $n_B(\lambda)$ from Figs. 3(a) and 3(b). Figures 4(b) and 4(c) present magnifications of the transmittance spectrum in color scale, respectively, around 500 nm and 1500 nm, both as functions of the wavelength and of the central-defect-layer refractive index (n_D). Observe the resonant peak at 513.26 nm for $n_D = 1$, and its shift towards the right side (long wavelength) of the stop band when n_D grows. At the same time, another resonant peak arises from the left side and crosses the stop band. Similar behavior is noted for the resonant peak around 1500 nm.

In Fig. 5, extra layer thickness (Δ_d) effects on the resonant peaks around (a) 500 nm and (a') 1500 nm are shown for the same FPC in Fig. 4 with $\Delta_d = 0$ nm (violet solid lines), $\Delta_d = 0.4$ nm (green open down triangles), and $\Delta_d = 0.8$ nm (orange open up triangles) added to each layer, as illustrated in Fig. 5(a"). Note the shifts in both resonant peaks towards long wavelengths.

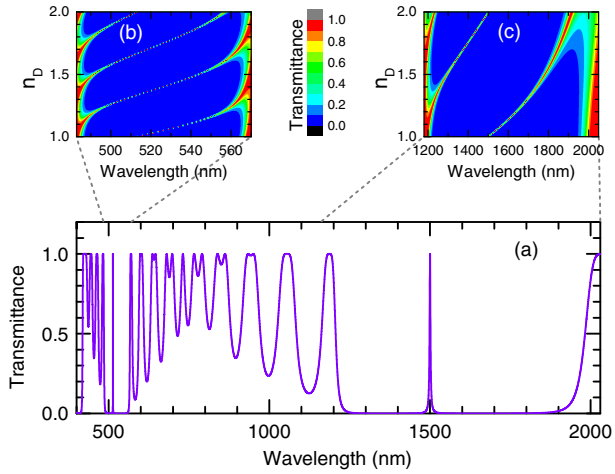

Fig. 4. (a) Transmittance spectrum obtained from *ab-initio* refractive indices for an FPC made of $(SiO_2 - TiO_2)^5 D (TiO_2 - SiO_2)^5$, and (b), (c) amplifications of (a), respectively, around 500 nm and 1500 nm, illustrating the resonance peak location as a function of n_D.

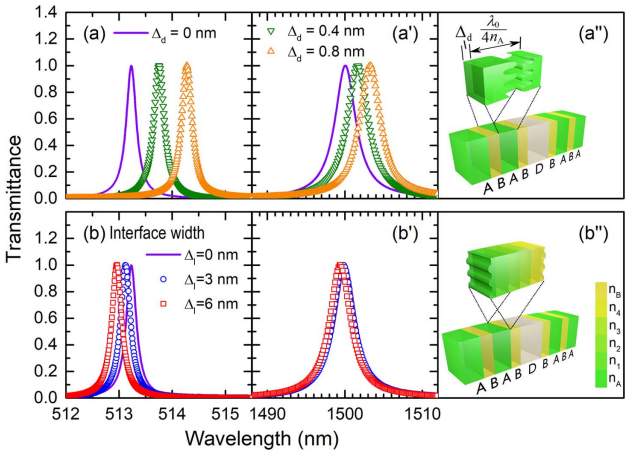

Fig. 5. Shifts in resonant peaks for the same FPC of Fig. 4 around (a), (b) 500 nm and (a'), (b') 1500 nm due to (a), (a') layer thickness addition (Δ_d) and (b), (b') interface width (Δ_I), both schematically drawn in Figs. 5(a"), (b").

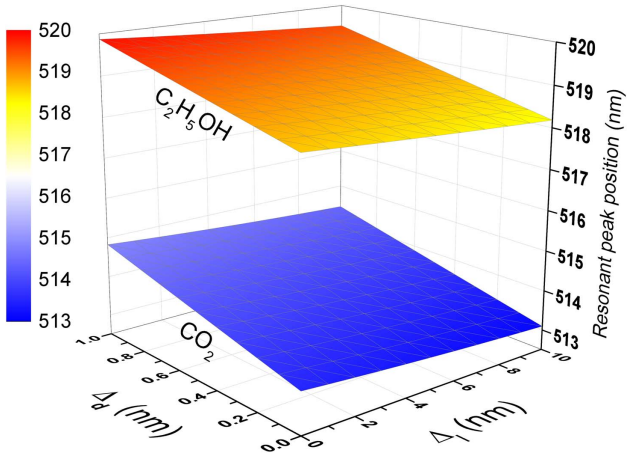

Fig. 6. Resonant peak wavelength around 500 nm as a function of the layer interface width (Δ_I) and extra layer thickness (Δ_d) for CO_2 and ethanol.

Displacements of resonant peaks around 500 nm and 1500 nm are, respectively, shown in Figs. 5(b) and 5(b') when a finite interface width (Δ_I) is considered for the same FPC in Fig. 4 with $\Delta_I = 0$ nm (violet solid lines), $\Delta_I = 3$ nm (blue open circles), and $\Delta_I = 6$ nm (red open squares). Figure 5(b") schematically illustrates such finite interface width modeled by four sublayers. It is worth mentioning that the resulting transmission spectra in Figs. 5(b) and 5(b') are essentially unchanged for sublayer numbers larger than four, and then only such almost-infinite-sublayer spectra are presented in Fig. 5.

Notice that the displacements of resonant peaks in Figs. 5(b) and 5(b') are smaller than those in Figs. 5(a) and 5(a') with an opposite direction, although the considered Δ_I is significantly larger than Δ_d, because the former does not break the quarter-wavelength condition. In addition, a detailed analysis of these transmission spectra reveals an almost constant FWHM of such analyzed main resonant peaks from these two cavity-structural perturbations.

Let us further analyze the functionality of a realistic FPC with the mentioned structural disorders by using it to measure the refractive indices of two compounds, such as CO_2 and ethanol (C_2H_5OH). When one of these compounds is introduced into the central vacuum space of the FPC, we should observe a shift in the measured resonant peak, which reveals the refractive index value of the compound. Figure 6 shows the variation of this resonant peak wavelength as a function of both the interface width (Δ_I) and the extra layer thickness (Δ_d) for CO_2 and ethanol.

Notice that the signs of these two variations are different, positive for Δ_d and negative for Δ_I, both with respect to a perfect FPC ($\Delta_I = \Delta_d = 0$). Moreover, these two surfaces in Fig. 6 are essentially parallel with an error less than 1%, which means that a unique relationship between the refractive index and the resonant peak shift can be used for the measurement of the refractive index. In other words, for two FPCs with different degrees of the analyzed structural disorders, which lead unlike initial resonant peak positions for the vacuum case, the refractive index of fluid can be obtained exclusively from the shift of this resonant peak.

In Fig. 7, the quality factors [13], defined as the ratio between the resonant peak wavelength and its FWHM, for CO_2 (blue rhombuses) and ethanol (red circles) are plotted versus the FPC layer number without structural disorder. When an interface width of 10 nm and an extra layer thickness of 1 nm from the quarter-wavelength condition are introduced into the FPC, the diminished quality factor values are shown by the error bars. The inset in Fig. 7 illustrates the resonant peaks of CO_2 from an FPC of 41 layers with (blue squares) and without (violet line) the structural disorders. Notice that the quality factor exponentially grows with the number of layers and slightly diminishes with the presence of structural disorders, due mainly to the increase in FWHM, as shown in the inset in Fig. 7. Observe a quality factor of 10^6 archived by an FPC of only 41 layers, even containing the mentioned structural disorders. This analysis reveals the robust performance of such an accurate FPC made of TiO_2 and SiO_2.

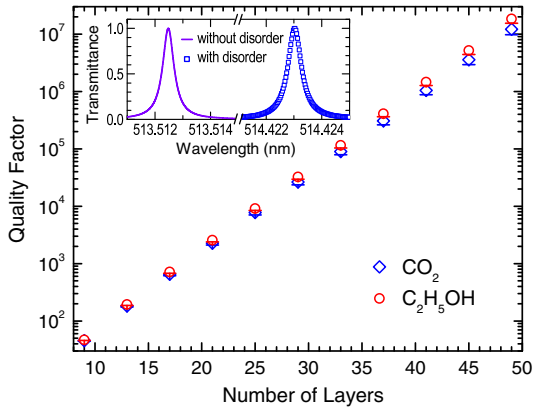

Fig. 7. Quality factor as a function of the FPC layer number for CO_2 (blue rhombuses) and ethanol (red circles), while diminished quality factor values of FPC with structural disorders are shown through the error bars. Inset: resonant peaks of CO_2 from an FPC of 41 layers with (blue squares) and without (violet line) the structural disorders.

5. CONCLUSIONS

We have presented a hybrid model by combining the quantum mechanics with the classical electromagnetism for the study and design of realistic FPCs. The refractive index obtained from a specific atomic arrangement by using the DFT was taken as the input of cavity optical property calculations through the transfer matrix method. This *ab-initio* hybrid model has the advantage of being simple and capable to predict macroscopic properties of devices. As an example, we have analyzed an FPC made of TiO_2/SiO_2 multilayers, whose optical transmittance has been studied in detail, including the effects of a finite layer interface width originated from the atomic diffusion at interface, as well as those derived from a possible systematic layer thickness variation.

The numerical results, partially verified by the analytical ones, reveal an exponential diminish of the FWHM with the layer number of the FPC and in consequence an exponential growth of the finesse, which ensures a high-quality FPC can be built by using tens of dielectric layers. However, there are other limitations, such as the refractive index contrast and the electronic band gap of the layers. In this sense, the DFT calculations can correlate these parameters with the atomic-scale structural arrangement and the chemical element election. Another important factor of a high-quality FPC is the structural purity. The results of this article show that a constant deviation of layer thickness around 0.4 nm (∼0.2%) can cause a shift of the main resonant peak larger than its FWHM. Hence, an accurate control during the FPC growth is truly crucial, as discussed in Ref. [2]. Nevertheless, the obtained results also indicate that neither a constant addition of the layer thickness nor the introduction of a finite interface width may produce a significant growth of the FWHM of the resonant peaks. This fact permits a reestablishment of the reference peak position in a real FPC with these two types of structural disorders and makes possible an accurate measurement of the refractive indices of gases and liquids. In summary, the FPC represents an accurate manner to determine the refractive indices of fluids, whose structure can be designed via the present hybrid method. This method can be carried out without the use of experimental data, allowing a wide-range search of new materials with high refractive index contrasts around the resonance frequency, which is fundamental for the fabrication of accurate FPCs.

Funding. Consejo Nacional de Ciencia y Tecnología (CONACYT) (252943).

Acknowledgment. We would like to thank Fernando Sánchez for his technical support and interesting discussions. This work has been partially supported by UNAM-PAPIIT-IN114916 and UNAM-PAPIIT-IN116317. Computations were performed at Miztli of DGTIC-UNAM.

REFERENCES

1. M. H. Bitarafan and R. G. DeCorby, "On-chip high-finesse Fabry–Perot microcavities for optical sensing and quantum information," Sensors **17**, 1748 (2017).
2. M. Vignaux, F. Lemarchand, C. Grezes-Besset, and J. Lumeau, "In situ optical monitoring of Fabry–Perot multilayer structures: analysis of current techniques and optimized procedures," Opt. Express **25**, 18040–18055 (2017).
3. M. S. Rauscher, M. Schardt, M. H. Köhler, and A. W. Koch, "Dual-channel mid-infrared sensor based on tunable Fabry–Perot filters for fluid monitoring applications," Sens. Actuators B Chem. **259**, 420–427 (2018).
4. P. Yeh, *Optical Waves in Layered Media* (Wiley, 2005), pp. 58–64 and 145-148.
5. N. B. Ali, "Optical Fabry-Perot filters using hybrid periodic, Fibonacci and Cantor photonic structures," Nano Commun. Netw. **13**, 34–42 (2017).
6. E. Maciá, "Exploiting aperiodic designs in nanophotonic devices," Rep. Prog. Phys. **75**, 036502 (2012).
7. M. D. Segall, P. J. D. Lindan, M. J. Probert, C. J. Pickcard, P. J. Hasnip, S. J. Clark, and M. C. Payne, "First-principles simulation: ideas, illustrations and the CASTEP code," J. Phys. Condens. Matter **14**, 2717–2744 (2002).
8. Y. Bonder and C. Wang, "A first-principles model of birefringent porous silicon," J. Appl. Phys. **100**, 044319 (2006).
9. S.-G. Park, B. Magyari-Köpe, and Y. Nishi, "Electronic correlation effects in reduced rutile TiO_2 within the LDA+U method," Phys. Rev. B **82**, 115109 (2010).
10. S. S. Nekrashevich and V. A. Gritsenko, "Electronic structure of silicon dioxide (a review)," Phys. Solid State **56**, 207–222 (2014).
11. M. C. Payne, M. P. Teter, D. C. Allan, T. A. Arias, and J. D. Joannopoulos, "Iterative minimization techniques for *ab-initio* total-energy calculations: molecular dynamics and conjugate gradients," Rev. Mod. Phys. **64**, 1045–1097 (1992).
12. R. Del Sole and R. Girlanda, "Optical properties of semiconductors within the independent-quasiparticle approximation," Phys. Rev. B **48**, 11789–11795 (1993).
13. B. E. A. Saleh and M. C. Teich, *Fundamentals of Photonics* (Wiley, 1991), p. 321.